



## How do nitrated lipids affect the properties of phospholipid membranes?

Maria C. Oliveira<sup>a</sup>, Maksudbek Yusupov<sup>b</sup>, Annemie Bogaerts<sup>b</sup>, Rodrigo M. Cordeiro<sup>a,\*</sup>

<sup>a</sup> Centro de Ciências Naturais e Humanas, Universidade Federal do ABC, Avenida dos Estados 5001, CEP 09210-580, Santo André, SP, Brazil

<sup>b</sup> Research Group PLASMANT, Department of Chemistry, University of Antwerp, Universiteitsplein 1, B-2610, Antwerp, Belgium

### ARTICLE INFO

#### Keywords:

Lipid nitro-oxidation  
Molecular dynamics simulations  
Isomers  
Lipid mixture

### ABSTRACT

Biological membranes are under constant attack of free radicals, which may lead to lipid nitro-oxidation, producing a complex mixture of nitro-oxidized lipids that are responsible for structural and dynamic changes on the membrane. Despite the latter, nitro-oxidized lipids are also associated with several inflammatory and neurodegenerative diseases, the underlying mechanisms of which remain elusive. We perform atomistic molecular dynamics simulations using several isomers of nitro-oxidized lipids to study their effect on the structure and permeability of the membrane, as well as the interaction between the mixture of these products in the phospholipid membrane environment. Our results show that the stereo- and positional isomers have a stronger effect on the properties of the membrane composed of oxidized lipids compared to that containing nitrated lipids. Nevertheless, nitrated lipids lead to three-fold increase in water permeability compared to oxidized lipids. In addition, we show that in a membrane consisting of combined nitro-oxidized lipid products, the presence of oxidized lipids protects the membrane from transient pores. It is well established that plasma application and photodynamic therapy produces a number of oxidative species used to kill cancer cells, through membrane damage induced by nitro-oxidative stress. This study is important to elucidate the mechanisms and the molecular level properties involving the reactive species produced during that cancer therapies.

### 1. Introduction

Lipid oxidation and lipid nitration are processes taking place in cell membranes, which result from an oxidative attack on the unsaturated acyl chains of lipids by *reactive oxygen and nitrogen species* (RONS), e.g., nitric oxide ( $^{\bullet}\text{NO}$ ), [1,2]. Lipid oxidation and nitration are involved in several diseases, such as atherosclerosis [3], cancer [4] and neurodegenerative disorders [5].

A number of experimental and computational studies have already demonstrated the effect of oxidation products (i.e., oxidized lipids) on the microscopic and macroscopic properties of the membrane, which results in structural changes related to the area per lipid, lipid order, bilayer thickness and bilayer hydration profile (see e.g. [6–9]). For instance, using the bilayer system composed of PLPC (1-palmitoyl-2-linoleoyl-*sn*-glycero-3-phosphatidylcholine) and its aldehyde and peroxide products, Boonnoy and co-workers observed the formation of water defects induced by both aldehyde and hydroperoxide lipids, where full pore formation was observed only in the bilayer consisting of aldehyde lipids. At 50% oxidation with aldehyde lipids, the pores were stable, however, at higher concentrations, the pores became unstable

and micellation occurred up to 1  $\mu\text{s}$  [10]. Furthermore, in another study the authors observed that alpha-tocopherols (vitamin E) not only protect the bilayer from oxidation but also help to stabilize the bilayer after lipid peroxidation (i.e., no pores were observed) [11].

In the same way, experimental and computational studies also revealed that nitrated fatty acids alter lipid organization by cluster formation at the membrane-water interface [12]. Moreover, nitrated phospholipids were detected in the cardiac mitochondria of diabetic rats treated with streptozotocin (a compound used to induce diabetes), and in the cardiomyocytes (cardiac muscle cells) under starvation using liquid chromatography coupled to a linear ion trap mass spectrometer, and were characterized by low energy collision-induced dissociation tandem mass spectrometry. These nitrated lipids showed anti-inflammatory and antioxidant properties, including the ability to inhibit lipid peroxidation [13–15]. Besides, nitrated POPC (1-palmitoyl-2-oleoyl-*sn*-glycero-3-phosphocholine) induced a series of downstream cellular effects, showing nitrated phospholipids as new potential electrophilic lipid mediators with selective actions [16].

Similar to as lipid oxidation, lipid nitration also leads to the formation of different nitration products with high yields, although the nitro

\* Corresponding author.

E-mail address: [rodrigo.cordeiro@ufabc.edu.br](mailto:rodrigo.cordeiro@ufabc.edu.br) (R.M. Cordeiro).

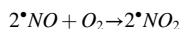
<https://doi.org/10.1016/j.abbi.2020.108548>

Received 23 June 2020; Received in revised form 23 July 2020; Accepted 19 August 2020

Available online 21 August 2020

0003-9861/© 2020 Elsevier Inc. All rights reserved.

phospholipid (NO<sub>2</sub>-PL) is one of the main nitrated lipids [13]. Nitric oxide (i.e., one of the RONS) diffuses into the hydrophobic core of biological membranes [17] as well as lipoproteins with a diffusion coefficient of  $2 \times 10^5 \text{ cm}^2 \text{ s}^{-1}$  [18], where it concentrates and reacts with O<sub>2</sub> to form nitrogen dioxide ( $\bullet\text{NO}_2$ ):



Herein, we present one possible pathway to lipid nitration (see Fig. 1). Nitrogen dioxide reacts with unsaturated lipids through a radical pathway involving a homolytic attack on the double bond, yielding a  $\beta$ -nitroalkyl radical, which at low oxygen concentration combines with other  $\bullet\text{NO}_2$  molecules to form nitro intermediates. The nitro group reduces electron density at the  $\beta$ -carbon of the double bond, leading to an increased reactivity with reaction products that have been detected in carcinogenic tissue, blood, and urine [19].

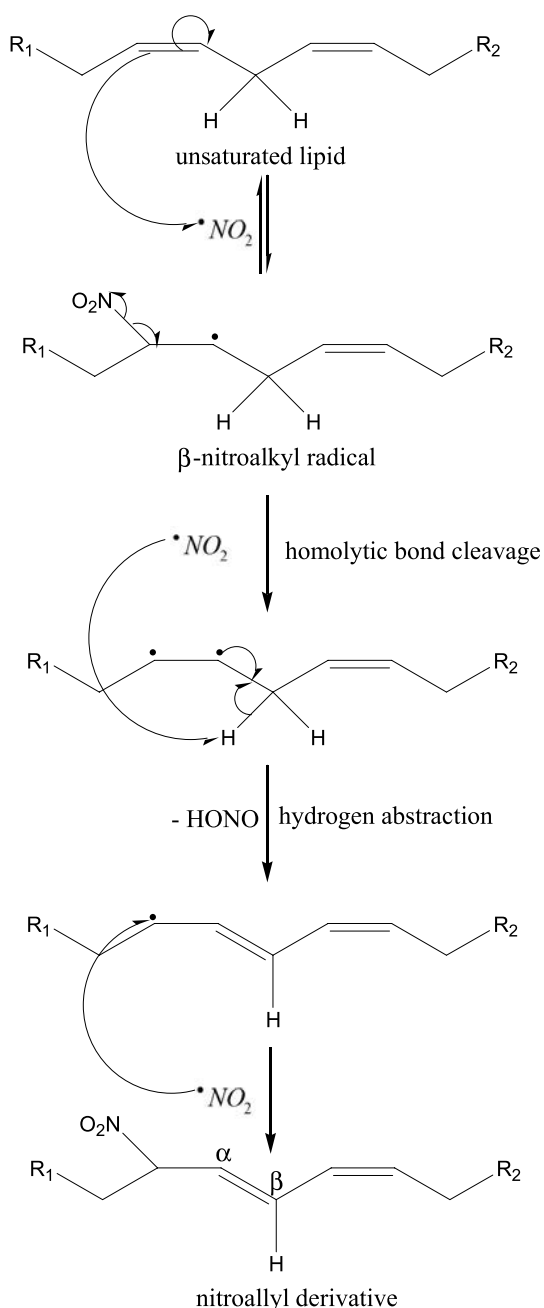


Fig. 1. Schematic representation of the lipid nitration mechanism by  $\bullet\text{NO}_2$  radical, where R<sub>1</sub> and R<sub>2</sub> represent acyl chains. Adopted from [19].

Besides, nitrite intermediates can also be formed producing nitroalkenes, while its hydrolysis yields nitro-alcohols. Since  $\bullet\text{NO}_2$  can also initiate lipid oxidation reactions, the nitration yield compared to oxidation depends on the O<sub>2</sub> level: at low concentrations of O<sub>2</sub>, the formation of nitrated products predominates, whereas under aerobic conditions, the lipid oxidation process is favored [20]. In addition, peroxyxynitrite anion (ONOO<sup>-</sup>) and peroxyxynitrous acid (ONOOH) are potent one- and two-electron oxidants, which mediate oxidation and nitration reactions. At physiological pH, ONOO<sup>-</sup> is in equilibrium with appreciable amounts of peroxyxynitrous acid (ONOOH; pK<sub>a</sub> = 6.5–6.8) [21] which can undergo homolysis of the O–O bond, thereby generating  $\bullet\text{NO}_2$  and the extremely reactive  $\bullet\text{OH}$  radical.

Furthermore, lipid nitro-oxidation, by addition or abstraction of hydrogen atoms, can result in different positional isomers [22]. For instance, in the case of linoleic acid (LA 18:2) at least three different nitrated products are formed, representing a mixture of stereo- and positional isomers [23]. Nevertheless, although several studies have been devoted to the investigation of different lipid oxidation products, there are few studies on the effect of lipid nitration products. Therefore, there is an urgent need for an improved understanding of the effect of lipid nitration on membrane properties, which is the subject of the present investigation.

As lipid oxidation products disturb the biophysical properties of biological membranes, it is reasonable to expect that lipid nitration can also affect the membrane structure and properties. Nevertheless, the physiological impact of nitrated lipids is still elusive. Thus, in this study, we aim to investigate through atomistic *molecular dynamics* (MD) simulations the effect of lipid nitration on the properties of phospholipid membranes composed of nitrated and/or oxidized POPC bilayers, using different stereo- and positional isomers.

## 2. Methods

### 2.1. Simulation systems

Atomistic MD simulations were performed applying the GROMACS 5.1.2 package [24]. All the systems were built using the Packmol software [25]. Graphical renderings of the simulated systems were produced using the VMD software [26]. In the following, we summarize the simulation protocol.

We simulated systems composed of POPC lipid molecules and their stable nitro-oxidation products at neutral pH, i.e., hydroperoxide (POPCOOH) and nitro (POPCNO<sub>2</sub>). The oxidation was considered at the C9 at *sn*-2 acyl chains with *R* or *S*-stereocenters (Fig. 2). We studied single-component homogeneous membranes as well as two-component heterogeneous membranes in a random mixture.

Each model membrane (or bilayer system) used in our MD simulations was composed of 128 lipids (64 lipid molecules per leaflet) surrounded by two water layers with a hydration level of  $\sim 46$  water molecules per lipid. In the case of the homogeneous membranes, each bilayer system consisted of either entirely POPC molecules (i.e., 100% POPC) or one of its nitro-oxidation products (i.e., 100% POPCOOH or 100% POPCNO<sub>2</sub>), whereas in the heterogeneous membranes, each system contained 50% POPCOOH and 50% POPCNO<sub>2</sub> molecules, equally and randomly distributed in each layer. As mentioned above, the POPCOOH and POPCNO<sub>2</sub> lipid molecules can have either *R* or *S* isomers (see Fig. 2). Water was modeled with the *simple point charge* (SPC) model [27]. The box used for the simulations was a rectangular box with periodic boundary conditions in all Cartesian directions.

Newton's equations of motion were integrated at intervals of 2 fs. Interatomic interactions were described according to the united-atom GROMOS 53A6 force field [28]. A cut-off radius of 1.4 nm was used for non-bonded (Lennard-Jones) and electrostatic (Coulomb) interactions. Coulomb interactions were treated using the *particle mesh Ewald* (PME) [29], based on the Ewald summation method. The covalent bond lengths were constrained using the LINCS algorithm [30].

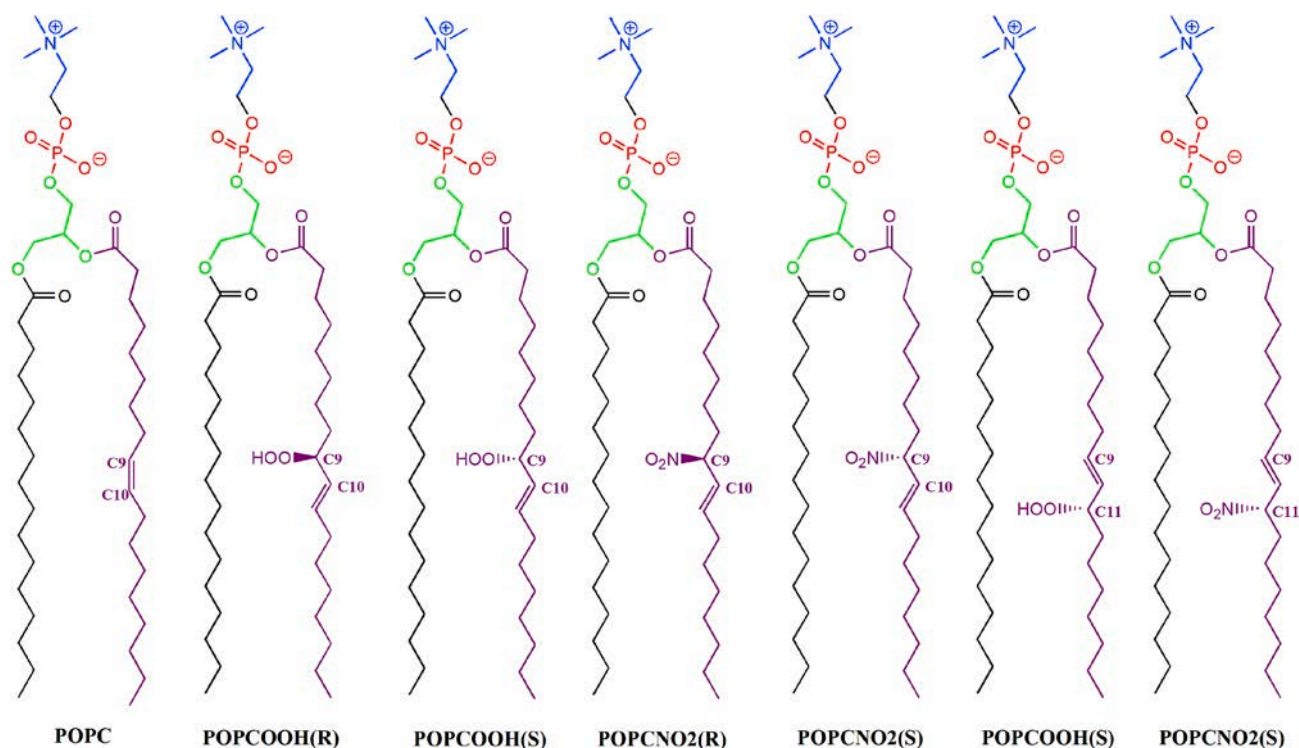


**Fig. 2.** Structures of the POPC molecule and the stereo- and positional isomers from its oxidation products simulated. The atoms in blue, red, and green represent choline, phosphate, and glycerol groups, respectively. The palmitoyl (*sn*-1) and oleoyl (*sn*-2) chains are represented by black and purple colors, respectively. R and S given in brackets denote the structure with R and S isomers, respectively. (For interpretation of the references to color in this figure legend, the reader is referred to the Web version of this article.)

A steepest descent energy minimization was performed prior to equilibration. Then, equilibration was performed applying the *isothermal-isobaric ensemble* (NPT) for at least 300 ns. The temperature was maintained close to the physiological temperature (310 K) by weakly coupling the system to an external temperature bath using a Nose-Hoover thermostat [31,32]. The temperature coupling relaxation time constant was 0.5 ps. The pressure was also maintained at around 1 bar by weakly coupling the system to an external pressure bath using a Parrinello-Rahman barostat [33]. The pressure coupling was applied semi-isotropically with a relaxation time constant of 2 ps, and isothermal compressibility of  $4.5 \times 10^{-5} \text{ bar}^{-1}$ .

## 2.2. Data analysis

The last 100 ns of each trajectory was used for analyses, with frames taken every 20 ps. We used the *gmx energy*, *gmx order*, *gmx density*, *gmx traj* and *gmx rdf* tools of the GROMACS programs to conduct data analysis.

The bilayer thickness was defined as the average distance along the *z*-axis between the center of mass of the phosphorus atoms of both leaflets. The area per lipid ( $A_L$ ) was calculated as:

$$A_L = \frac{L_x \times L_y}{n_L} \quad (1)$$

where  $L_x$  and  $L_y$  are the box length in the *x* and *y*-direction, respectively, and  $n_L$  is the number of lipids in each leaflet (i.e., 64).

The lipid acyl chain deuterium order parameters ( $S_{CD}$ ), i.e., the measure of the orientation mobility of the C–D bond, was calculated as:

$$S_{CD} = \left\langle \frac{3\cos^2\theta_{z,i} - 1}{2} \right\rangle \quad (2)$$

where  $\theta_{z,i}$  is the angle between the C–D (C–H in the present simulations) bond vector of a carbon atom *i* and the bilayer normal (*z*-direction). The

brackets indicate the ensemble average. The average is taken for all lipids over both C–D bonds of a  $\text{CD}_2$  group, for each C-atom of the *sn*-1 and *sn*-2 chain over time.

The free energy ( $\Delta G$ ) barrier associated with the transport of a water molecule from a distant point in solution to a specific position *z* inside the membrane, was calculated using the Boltzmann equation:

$$\Delta G(z) = -k_B T \ln \frac{\rho(z)}{\rho_\infty} \quad (3)$$

where  $k_B$  is the Boltzmann constant, *T* is the temperature,  $\rho(z)$  is the distance-dependent number density of water molecules, and  $\rho_\infty$  its bulk value.

## 3. Results and discussion

### 3.1. Parametrization of the nitration products

Well-validated models were used for the description of unsaturated lipids [34] and lipid hydroperoxides [35], as well as for other lipid oxidation products containing alcohol, ketone, and aldehyde functional groups taken from the standard GROMOS 53A6 force field library [28, 36]. However, given the large variety of lipid oxidation and nitration products, we might investigate lipid nitro-oxidation products with functional groups that are currently missing in the force field library [37, 38].

For this purpose, the interaction parameters for nitration products, using the R and S isomers from the molecule 3-nitro-1-butene as nitrated lipid fragment, were developed from electronic structure calculations applying the Gaussian 09 software [39]. Parameters for the bonds, angles, and torsional potentials at the C–C–N–O fragments were optimized performing DFT calculations (B3LYP functional with the 6-311++g (d, p) basis set) in vacuum, by scanning their conformational energy surfaces. Using the CHELPG scheme, sets of atom-centered partial charges

were obtained by fitting the electrostatic potentials obtained from quantum and classical mechanical calculations. Atom-centered point charges of  $+0.67e$  and  $-0.44e$  were considered for nitrogen and oxygen, respectively. The parameters of the Van der Waals interactions were selected from available force field libraries, to keep consistency with the chosen membrane models.

Fig. 3 represents the fitting of the standard potential energy function to the quantum mechanical energy. Using this energy function we obtained the parameters of the C–C–N–O dihedral angle for both *R* and *S* isomers of 3-nitro-1-butene. Similar fitting procedures were performed for obtaining the bond and angle parameters (i.e., for the calculation of bond and angle force constants).

To evaluate how well the parameters (obtained by fitting) represent the quantum model, an equilibration simulation was performed for 50 ns applying the *canonical ensemble* (NVT) at 1 bar and 298 K, for computation of its dihedral angle distribution. The results are summarized in Fig. S1. It was found that the distributions from the *S* isomer were very similar to quantum calculations, showing two-fold symmetric distribution. On the other hand, integrating the distribution for the *R* isomer gave the proportion under each peak to be 47.6% and 52.4%, i.e., an asymmetric distribution. Nevertheless, the difference between quantum and classical average energies was very similar for both *R* and *S* isomers:  $0.4180 \text{ kJ mol}^{-1}$  and  $-0.4113 \text{ kJ mol}^{-1}$ , respectively.

Thus, we obtained new GROMOS 53A6 force field parameters for bonds, angles and dihedral angle of the  $\text{NO}_2$  functional group (i.e., nitration product, see Fig. 3) by fitting some potential energy functions to the DFT energies. These parameters were used in our further MD simulations (see sections below). More information about the newly obtained parameters is given in Supplementary Material.

### 3.2. Convergence of membrane properties

We evaluated the membrane properties, such as area per lipid and bilayer thickness, as a function of simulation time (see Fig. S2a). At 310 K, the convergence of all properties was observed within hundreds of nanoseconds among the investigated systems. The calculated average area per lipid using the last 100 ns of simulation was  $0.616 \pm 0.008 \text{ nm}^2$  for the POPC bilayer system (see Fig. 4a). It is comparable with the value of  $0.662 \pm 0.013 \text{ nm}^2$ , obtained by experiments from solid-state  $^2\text{H}$  NMR spectroscopy [40]. The bilayer systems containing POPCOOH(*R*) and POPCOOH(*S*) lipids presented an area per lipid of  $0.712 \pm 0.010 \text{ nm}^2$  and  $0.693 \pm 0.010 \text{ nm}^2$ , respectively, which is around 15% higher than that for native POPC bilayer. The latter is in agreement with experimental measures of POPCOOH using a micropipette setup coupled to an epi-fluorescence microscope, where an increase of roughly 15–20% in the area per lipid was observed [41].

Similar values of the area per lipid were obtained for POPCNO2(*R*)

and POPCNO2(*S*) systems, i.e.,  $0.712 \pm 0.013$  and  $0.702 \pm 0.012 \text{ nm}^2$ , respectively. As is clear, both POPCOOH and POPCNO2 systems presented a higher area per lipid compared to the native POPC system, and it was even higher for systems with *R* isomers (see Fig. 4a).

Regarding the bilayer thickness, the nitro-oxidation decreased the bilayer thickness by around 0.40 nm when compared to the native POPC system (see Fig. 4a). The POPCOOH(*S*) bilayer thickness was around 0.10 nm higher compared to POPCOOH(*R*), while the POPCNO2(*S*) bilayer thickness was around 0.05 nm higher compared to POPCNO2(*R*).

### 3.3. Effect of the double bond's position on structural properties

During the lipid oxidation, when singlet oxygen is added directly to unsaturated carbon by an *ene* addition reaction, it results in a change either in the stereo- or position of the double bond. To evaluate how the position of the double bond affects membrane properties, we simulated the nitro-oxidized systems by changing the position of the double bond. In other words, we added the C=C double bond at C9 and the functional group at C11 (cf. Fig. 2). The results are presented in Fig. 4b.

Interestingly, for the POPCOOH(*S*) system, the area per lipid increased when the double bond was added before the –OOH group (i.e., at C9), revealing that the double bond facilitates the migration of the –OOH group towards the membrane surface. For the POPCNO2(*S*) system, on the other hand, we did not observe the positional effect of the C=C double bond (Fig. 4b). Several studies have already shown that oxidation increases the area per lipid due to the migration of the polar group –OOH to the hydrophilic membrane surface, leading to a decrease in the bilayer thickness [42–44]. Hence, the bilayer becomes thinner, thereby increasing its permeability. However, the question arises: why does this not apply to the –NO<sub>2</sub> group? To answer this question, we calculated the *radial distribution function* (RDF) to find out which groups are located near the –NO<sub>2</sub> group (Fig. 5).

Analysis of the RDF of the –OOH groups for the POPCOOH(*R*) system showed that the first peak appears at 0.168 nm, which belongs to carbonyl ester groups. On the other hand, the RDF of the –NO<sub>2</sub> groups for the POPCNO2(*S*) system showed a broad first peak starting at about 0.569 nm and with a maximum at about 0.973 nm for carbonyl ester groups. This means that the –OOH groups are closer to carbonyl ester groups than the –NO<sub>2</sub> groups, which is due to a strong dipole-dipole interaction between the groups.

Analysis of the distance from the phosphate groups showed the first peak appearing at 0.166 nm for the –OOH groups, which starts at about 0.430 nm and with a maximum at about 1.379 nm for the –NO<sub>2</sub> groups. Hence, the –OOH groups are more close to the phosphate groups compared to the –NO<sub>2</sub> groups. Both functional groups are at almost the same distance from the amine groups, i.e., the peaks are at 0.364 nm and 0.389 nm for –OOH and –NO<sub>2</sub>, respectively.

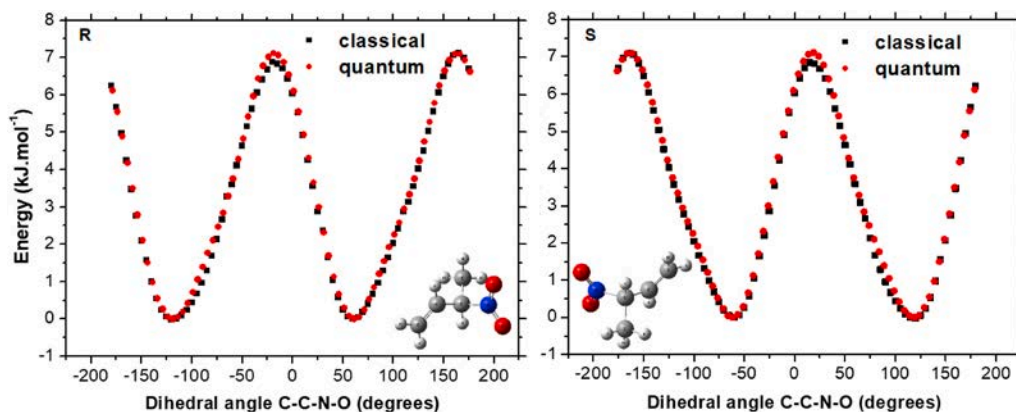


Fig. 3. Fitting of the standard potential energy function used for the C–C–N–O dihedral angle to the DFT energy, calculated for both *R* and *S* isomers of 3-nitro-1-butene.



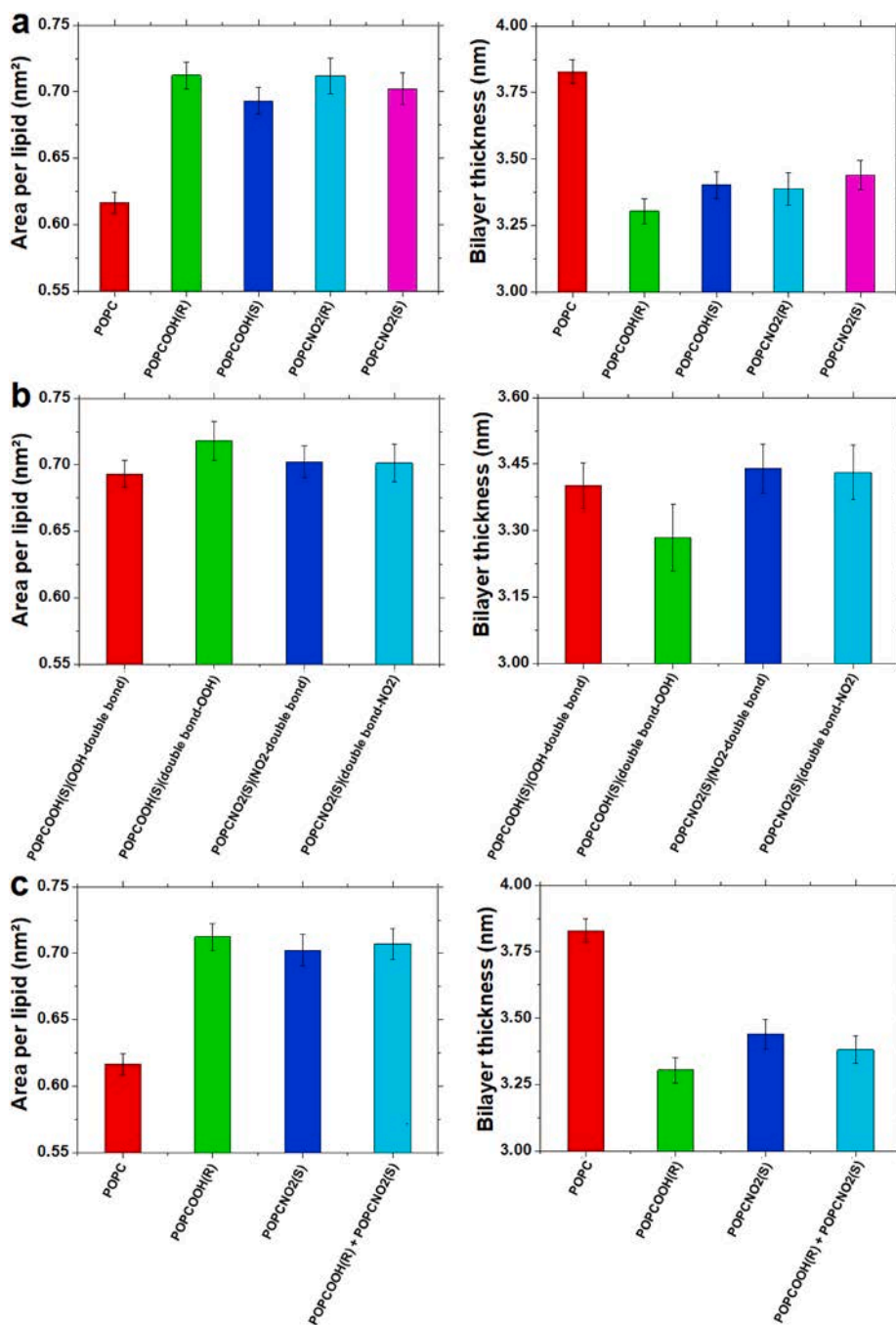


Fig. 4. Area per lipid and bilayer thickness calculated for different bilayer systems. The values are averaged from the last 100 ns of simulation.

Although the  $-OOH$  groups are approximately at the same distance from the phosphate and carbonyl ester groups, there are more molecules of the carbonyl ester groups surrounding the  $-OOH$  groups compared to the phosphate groups (see Fig. 5). Besides, there are almost two times higher amine groups close to the  $-OOH$  groups compared to the  $-NO_2$  groups. These results suggest that the  $-OOH$  groups prefer to interact with the membrane surface (i.e., with the head group components) and the  $-NO_2$  groups prefer to stay inside the membrane interior, which is clear from Fig. 6a. This phenomenon caused the *sn*-2 chains of the POPCOOH(R) system to bend towards the headgroup region, thereby increasing the lipid disorder. Despite the area per lipid also increased for POPCNO2(S), the *sn*-2 chain remained close to the native POPC system (see Fig. S3).

As a consequence of the migration of  $-OOH$  groups to the membrane

surface, the total density at the membrane interior decreased, and the membrane became more susceptible to pore formation. Indeed, the calculated density profile showed that the  $-OOH$  groups are closer to the P atoms (membrane surface) compared to the  $-NO_2$  groups (see Fig. 7a and b). Although no pore formation was observed within the time scale of our simulations (i.e., 300 ns), the density profile of the POPCNO2(S) system showed that the water density at the bilayer center increased by three times compared to the POPCOOH(R) system (Fig. 7d). It suggests that  $-NO_2$  groups might facilitate water molecules to transport into the bilayer center when remaining at the membrane interior. This will be discussed in detail in the sections below.

Thus, in summary, we found that the position of the C=C double bond plays a role in the structural properties of the membrane containing oxidized lipids. The  $-OOH$  groups remained more close to the

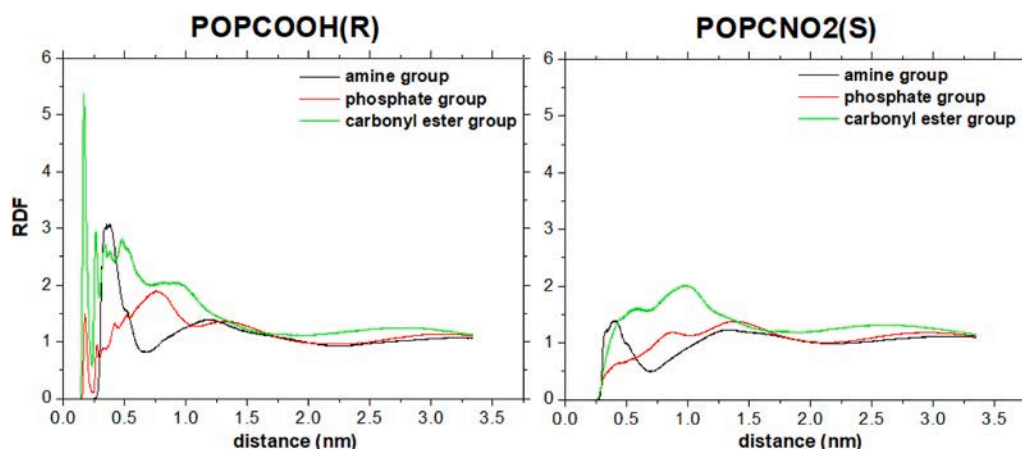


Fig. 5. Radial distribution function calculated for  $-OOH$  and  $-NO_2$  groups using the last 100 ns of simulation. The functional groups were added at C9 and the C=C double bond at C10.

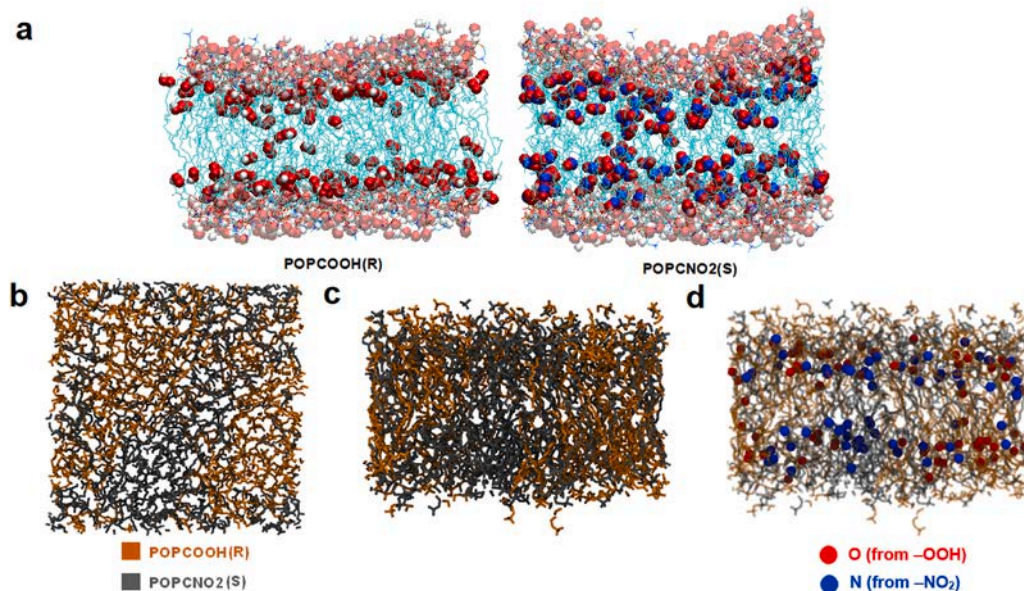


Fig. 6. Snapshots from MD simulations taken at 300 ns for the POPCOOH and POPCNO2 systems. (a) Side view of the POPCOOH(R) and POPCNO2(S) membranes, where the acyl chains are represented as cyan lines and water molecules as pale van der Waals spheres. Oxygen, hydrogen, and nitrogen atoms are represented as red, white, and blue van der Waals spheres, respectively. (b) Top view of combined nitro-oxidized membrane (i.e., containing both POPCOOH and POPCNO2 lipids), where the acyl chains are represented as solid lines. (c) Side view of the same system as shown in (b). (d) Side view of the same system as shown in (b), where the oxygen and nitrogen atoms are represented as red and blue van der Waals spheres, respectively. (For interpretation of the references to color in this figure legend, the reader is referred to the Web version of this article.)

bilayer surface compared to the  $-NO_2$  groups. Moreover, the nitrated lipids facilitated water molecules to transport into the bilayer center.

### 3.4. Combined effect of nitro-oxidation products

Lipid oxidation leads to a complex mixture of lipid nitro-oxidation products, which in turn have different effects on the membrane structure. Recently, we investigated the effects of mechanical stress on oxidized phospholipid bilayers, and we demonstrated that the presence of coexisting non-oxidized and oxidized domains decreased the areal strain for pore formation [45].

To evaluate the mixture of lipid nitro-oxidation products, we performed MD simulations of the POPCOOH(R):POPCNO2(S) (1:1) system, starting from random distribution of the lipids, which leads to a mixed POPCOOH(R)+POPCNO2(S) system after equilibration (see Fig. 6b and c). The time evolution of the area per lipid and bilayer thickness is given in Fig. S2c and the average area per lipid was found to be around  $0.707 \pm 0.011 \text{ nm}^2$  (Fig. 4c). Interestingly, the combination of the nitro-oxidized lipid components demonstrated that the presence of  $-OOH$  groups facilitated a higher migration of  $-NO_2$  groups to the membrane surface (Fig. 6d), compared to the system composed of only  $-NO_2$  containing lipids. Subsequently, the  $-NO_2$  groups remained more close to

the water molecules (Fig. 7c). Nevertheless, the water density in the bilayer center was very similar to the POPCOOH(R) system, i.e., about three times less than in the POPCNO2(S) system (Fig. 7d). Taken together, the simulation results suggest that the combined nitro-oxidized membrane system is less permeable to water molecules compared to the POPCNO2(S) system (Fig. 7d).

### 3.5. Effect of nitro-oxidation on the permeability of membrane

It is well known that lipid oxidation may lead to poration and leakage, and our last studies showed that the oxidation decreases the free energy barrier to water permeation, especially in membranes with aldehyde groups due to their shorter and highly mobile tail [46]. To investigate why the water density at the center of the bilayer was higher in the POPCNO2(S) system than in the POPCOOH(R), we calculated the number of water molecules across the membrane using the last 150 ns simulation time (Fig. 8). The software for analysis was developed by the research group of Prof. Dr. Alexandre Suman de Araujo from IBILCE/UNESP.

During the last 150 ns of simulation, we counted 3 permeation events for POPC, 7 for POPCOOH(R) and 20 for POPCNO2(S). This means that the POPCOOH(R) system is approximately two times more permeable

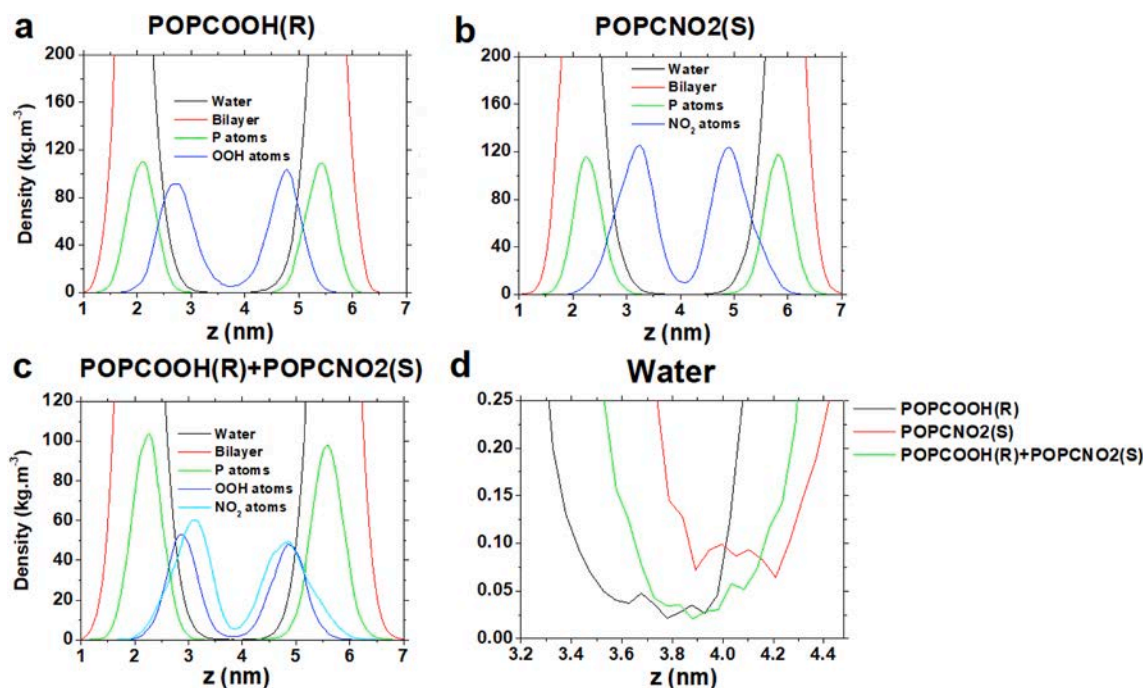


Fig. 7. Density profiles of different components of the membrane obtained using the last 100 ns of simulation.

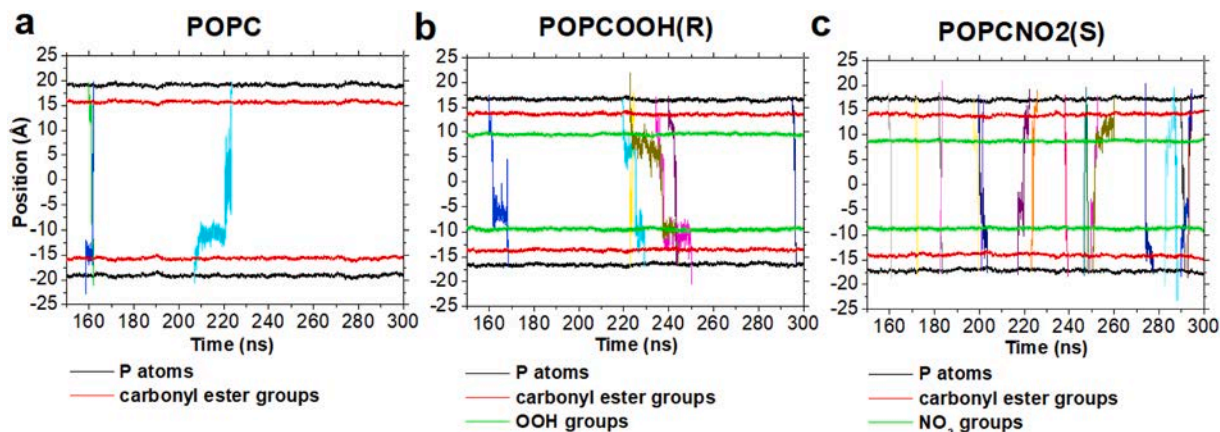


Fig. 8. Number of water permeation events calculated over the last 150 ns of MD simulation for (a) POPC, (b) POPCOOH(R) and (c) POPCNO2(S) membrane systems. The positions of some atoms and functional groups of the membranes (over time) are presented in different colors (black, red and green; see legend). The other colors represent the permeation events of water molecules, which start from the upper P atom (corresponding to the upper water layer) till the lower P atom (corresponding to the lower water layer, see black lines). (For interpretation of the references to color in this figure legend, the reader is referred to the Web version of this article.)

for water than native POPC, and the POPCNO2(S) is approximately three times more permeable than POPCOOH(R) and about 7 times more permeable than the POPC system. As is clear from Fig. 8, water molecules spent more time around the  $-OOH$  group region in the POPCOOH(R) system (see Fig. 8b) than around the  $-NO_2$  group region in the POPCNO2(S) system (see Fig. 8c). Both  $-OOH$  and  $-NO_2$  groups can form hydrogen bonds with water molecules, and this might explain the water trapping in the region around these groups.

The calculated average number of hydrogen bonds for  $-OOH$  and  $-NO_2$  groups are presented in Fig. 9. As is clear, the  $-OOH$  groups could act as both donor and acceptor of hydrogen bonds, whereas the  $-NO_2$  groups acted only as an acceptor. The  $-OOH$  groups as donors established more hydrogen bonds with carbonyl ester groups than with water molecules. This might explain the preserved membrane integrity observed by experiments in fully hydroperoxidized membranes [41]. Interestingly, the  $-NO_2$  groups as acceptors were able to establish

considerably more hydrogen bonds with water molecules than the  $-OOH$  groups. Thus, we can speculate that the strong interaction of  $-OOH$  groups with carbonyl ester groups prevents the diffusion of water into the core of the membrane. This is not the case for  $-NO_2$  groups, as they form hydrogen bonds only with water molecules, thereby facilitating the diffusion of water through the membrane.

To summarize, the nitro ( $-NO_2$ ) groups are more susceptible to transport water molecules into the membrane interior than the hydroperoxide ( $-OOH$ ) groups. Moreover, in the nitro groups the negative charge is stabilized by electronic delocalization (resonance), resulting in a weak base. In other words, the nitro groups become a higher acceptor of hydrogen bonds compared to ketone groups (which also act as acceptors). That could explain why the membrane permeability was preserved in membranes that contain ketone groups as an oxidation product [46].

To verify the latter hypothesis and simulate the electronic



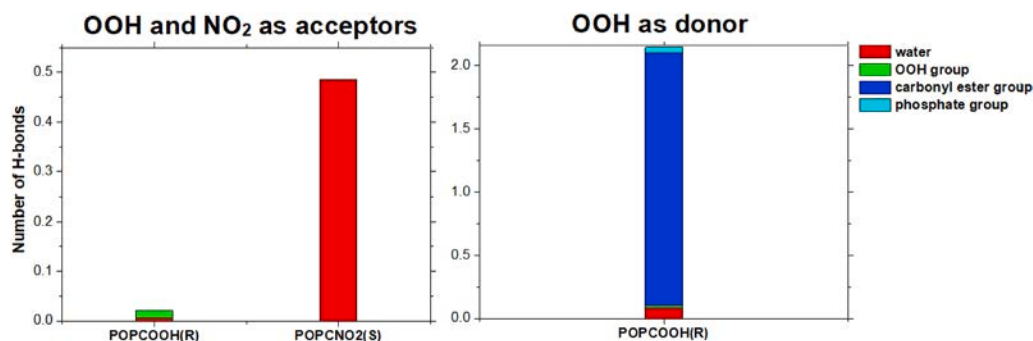


**Fig. 9.** Average number of hydrogen bonds established between the  $-OOH$  and  $-NO_2$  groups, with water or with the  $-OOH$ , carbonyl ester or phosphate groups of the membrane (see legend), with  $-OOH$  and  $-NO_2$  acting either as acceptor or donor. The number of bonds was defined at a maximum distance of 0.25 nm for the acceptors and averaged over the last 150 ns of the simulation.

delocalization present in the nitro group, we performed extra MD simulations using a system composed of oxidized POPC with a ketone group (POPCO), where the charge of the oxygen atom from the ketone group was increased from  $-0.45e$  to  $-0.65e$ . The results showed that the POPCO membrane presented more fluctuations and the water permeability was very similar to POPCNO<sub>2</sub>(S) (22 permeation events). Moreover, the carbonyl ester groups remained closer to the oxygen atoms of the ketone groups and the water molecules spent more time at the bilayer center (Fig. S4).

This might explain why nitro groups are a better water transporter to the membrane interior than ketone groups: lipid nitro-oxidation products with highly charged groups lead to an increase in the membrane permeability. It must be noted that this last simulated system is not a realistic representation, it is only used to demonstrate or refute our hypothesis.

Finally, to make a rough estimation of the energy necessary to transport water to the membrane interior, the free energy barrier ( $\Delta G$ ) was calculated using the Boltzmann equation [47]. In agreement with our previous results (Fig. 8), in the oxidized system with  $-OOH$  containing lipids the free energy barrier to water permeation decreased by approximately  $3 \text{ kJ mol}^{-1}$  compared to the native POPC system, whereas in the nitrated membrane with  $-NO_2$  containing lipids it decreased by approximately  $6 \text{ kJ mol}^{-1}$  (see Fig. 10). Hence, the membranes with nitrated lipids are more susceptible to pore formation than the membranes with oxidized lipids. The free energy barrier obtained for the membrane system with combined nitro-oxidized lipids was similar as for the oxidized membrane (see Fig. 10).

Transmembrane water permeation follows the solubility-diffusion model [48]. Water molecules first partition from the aqueous phase

into the membrane, a process associated with a steep free energy rise (c. f. POPC data in Fig. 10). Once inside the membrane, water molecules diffuse in a nearly flat energy landscape. In this scenario, we can expect nitro-oxidation to affect water permeability in many ways, which include: i) enhancement of the water-to-membrane partition coefficient due to increased membrane polarity; ii) change of the intramembrane diffusion coefficient of water; iii) shortening of the intramembrane diffusion path due to decreased membrane thickness. From all these effects, the partition free energy is expected to be dominant because permeability is exponentially dependent on it [49]. In fact, given the uncertainties of the free energy profiles in Fig. 10, the decrease of  $\sim 5 \text{ kJ mol}^{-1}$  in the permeation barrier is more than enough to explain the larger permeability of nitrated lipids as compared to their native counterparts.

#### 4. Conclusions

We performed atomistic MD simulations for evaluating the influence of nitro ( $-NO_2$ ) groups and their isomers as nitration products in phospholipid on the membrane properties, comparing the results with those for an oxidized membrane containing hydroperoxide groups. The simulations revealed that both stereo- (*R* and *S* isomers) and position isomers (i.e., changing the position of the functional group and C=C double bond) have a higher impact on oxidized lipids than for nitrated lipids. Nevertheless, the water permeability for nitrated lipids increased by three-fold compared to oxidized lipids. We also analyzed the influence of combined lipid nitro-oxidation products and found that the presence of oxidized lipids protects the membrane from transient pores, suggesting a synergistic effect between nitro-oxidized lipids. Thus, we must not

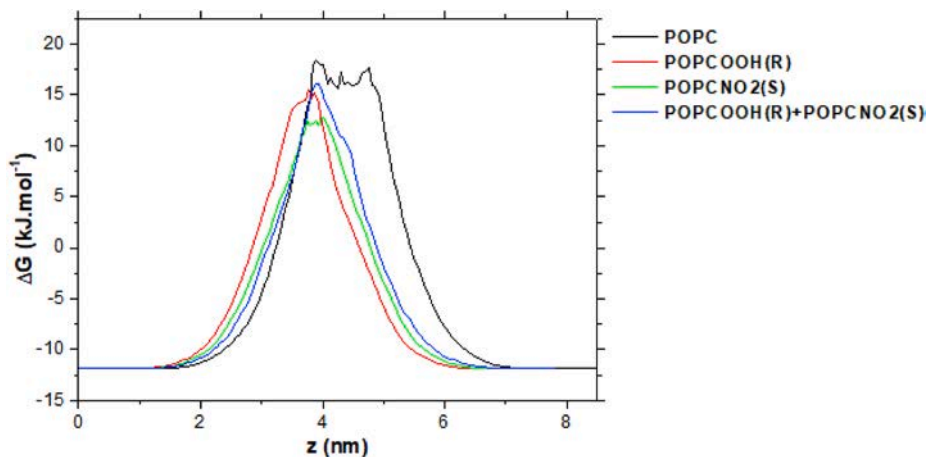


**Fig. 10.** The free energy barrier for permeation of water across different membrane systems, calculated using the last 100 ns of simulation. The functional groups were added at C9 and the C=C double bond at C10.



consider only the nitrated or oxidized membrane alone, but also the mixture between different nitro-oxidized lipids.

Our study provides reliable atomistic details about the role of nitrated lipids and the mixture of nitro-oxidized lipids in model membranes at different isomeric states, which is of interest for, e.g., the application of *cold atmospheric plasmas* (CAPs) in cancer treatment. This therapy produces a large number of extracellular RONS, which may diffuse into cancer cells significantly faster than into normal counterparts upon the same treatment with CAPs. Hence, these RONS are able to cause nitro-oxidative stress in the interior of the cell, inducing proapoptotic factors. Moreover, it will also be of great interest to other cancer therapies, such as chemotherapy, radiotherapy, and photodynamic therapy [50].

## Acknowledgements

We thank Universidade Federal do ABC for providing the computational resources needed for completion of this work and CAPES for scholarship granted. M.Y. acknowledges the Flanders Research Foundation (grant 1200219N) for financial support.

## Appendix A. Supplementary data

Supplementary data to this article can be found online at <https://doi.org/10.1016/j.abb.2020.108548>.

## References

- A. Ayala, M.F. Muñoz, S. Argüelles, Lipid peroxidation: production, metabolism, and signaling mechanisms of malondialdehyde and 4-hydroxy-2-nonenal, *Oxidative Med. Cell. Longev.* 2014 (2014) 360438.
- H. Yin, L. Xu, L.N.A. Porter, Free radical lipid peroxidation: mechanisms and analysis, *Chem. Rev.* 111 (2011) 5944–5972.
- J.A. Berliner, N. Leitinger, et al., The role of oxidized phospholipids in atherosclerosis, *JLR (J. Lipid Res.)* 50 (2009) S207–S212.
- R.P. Wu, T. Hayashi, H.B. Cottam, G. Jin, S. Yao, C.C.N. Wu, M.D. Rosenbach, M. Corr, R.B. Schwab, D.A. Carson, Nrf2 responses and the therapeutic selectivity of electrophilic compounds in chronic lymphocytic leukemia, *Proc. Natl. Acad. Sci. Unit. States Am.* 107 (2010) 7479–7484.
- M.A. Bradley-Whitman, M.A. Lovell, Biomarkers of lipid peroxidation in Alzheimer disease (AD): an update, *Arch. Toxicol.* 89 (2015) 1035–1044.
- L. Beranova, L. Cwiklik, et al., Oxidation changes physical properties of phospholipid bilayers: fluorescence spectroscopy and molecular simulations, *Langmuir* 26 (2010) 6140–6144.
- M.A.A. Ayee, E. LeMaster, et al., Molecular-scale biophysical modulation of an endothelial membrane by oxidized phospholipid, *Biophys. J.* 112 (2017) 325–338.
- M. Yusupov, K. Wende, S. Kupsch, et al., Effect of head group and lipid tail oxidation in the cell membrane revealed through integrated simulations and experiments, *Sci. Rep.* 7 (2017) 5761.
- M. Yusupov, J. Van der Paal, E.C. Neyts, A. Bogaerts, Synergistic effect of electric field and lipid oxidation on the permeability of cell membranes, *Biochim. Biophys. Acta Gen. Subj.* 1861 (2017) 839–847.
- P. Boonnoy, V. Jarerattanachai, M. Karttunen, J. Wong-ekkabut, Bilayer deformation, pores, and micellation induced by oxidized lipids, *J. Phys. Chem. Lett.* 6 (2015) 4884–4888.
- P. Boonnoy, M. Karttunen, J. Wongekkabut, Alpha-tocopherol inhibits pore formation in oxidized bilayers, *Phys. Chem. Chem. Phys.* 19 (2017) 5699–5704.
- J. Franz, T. Bereau, S. Pannwitt, et al., Nitrated fatty acids modulate the physical properties of model membranes and the structure of transmembrane proteins, *Chem. Eur. J.* 23 (2017) 9690–9697.
- T. Melo, P. Domingues, R. Ferreira, I. Milic, et al., Recent advances on mass spectrometry analysis of nitrated phospholipids, *Anal. Chem.* 88 (2016) 2622–2629.
- T. Melo, P. Domingues, T.M. Ribeiro-Rodrigues, H. Girão, et al., Characterization of phospholipid nitrooxidation by LC-MS in biomimetic models and in H9c2 Myoblast using a lipidomic approach, *Free Radical Biol. Med.* 106 (2017) 219–227.
- T. Melo, S.S. Marques, I. Ferreira, M.T. Cruz, et al., New insights into the anti-inflammatory and antioxidant properties of nitrated phospholipids, *Lipids* 53 (2018) 117–131.
- S. Duarte, T. Melo, R. Domingues, J. de Dios Alché, et al., Insight into the cellular effects of nitrated phospholipids: evidence for pleiotropic mechanisms of action, *Free Radical Biol. Med.* 144 (2019) 192–202.
- J. Razzokov, M. Yusupov, R.M. Cordeiro, A. Bogaerts, Atomic scale understanding of the permeation of plasma species across native and oxidized membranes, *J. Phys. Appl. Phys.* 51 (2018) 365203.
- M. Moller, H. Botti, C. Batthyany, H. Rubbo, R. Radi, A. Denicola, Direct measurement of nitric oxide and oxygen partitioning into liposomes and low density lipoprotein, *J. Biol. Chem.* 280 (2005) 8850–8854.
- A. Trostchansky, H. Rubbo, Nitrated fatty acids: mechanism of formation, chemical characterization and biological properties, *Free Radical Biol. Med.* 44 (2008) 1887–1896.
- V.B. O'Donnell, B.A. Freeman, Interactions between nitric oxide and lipid oxidation pathways: implications for vascular disease, *Circ. Res.* 88 (2001) 12–21.
- W.H. Koppenol, P.L. Bounds, T. Nausner, R. Kissner, H. Rügger, Peroxynitrous acid: controversy and consensus surrounding an enigmatic oxidant, *Dalton Trans.* 41 (2012) 13779–13787.
- P.R. Baker, F.J. Schopfer, S. Sweeney, B.A. Freeman, Red cell membrane and plasma linoleic acid nitration products: synthesis, clinical identification, and quantitation, *Proc. Natl. Acad. Sci. U.S.A.* 101 (2004) 11577–11582.
- V.B. O'Donnell, J.P. Eiserich, P.H. Chumley, M.J. Jablonsky, et al., Nitration of unsaturated fatty acids by nitric oxide-derived reactive nitrogen species peroxynitrite, nitrous acid, nitrogen dioxide, and nitronium ion, *Chem. Res. Toxicol.* 12 (1999) 83–92.
- M.J. Abraham, T. Murtola, R. Schulz, S. Páll, J.C. Smith, B. Hess, E. Lindahl, GROMACS: high performance molecular simulations through multi-level parallelism from laptops to supercomputers, *Software* 1 (2015) 19–25.
- L. Martinez, R. Andrade, E.G. Birgin, J. M. Martinez Packmol, A package for building initial configurations for molecular dynamics simulations, *J. Comput. Chem.* 30 (2009) 2157–2164.
- W. Humphrey, A. Dalke, K. Schulten, VMD: visual molecular dynamics, *J. Mol. Graph.* 14 (1996) 33–38.
- H.J.C. Berendsen, et al., Interaction models for water in relation to protein hydration, in: *Intermolecular Forces*, B. Pullman, Dordrecht, 1981, pp. 331–342.
- C. Oostenbrink, A. Villa, et al., A biomolecular force field based on the free enthalpy of hydration and solvation: the GROMOS force-field parameter sets 53A5 and 53A6, *J. Comput. Chem.* 25 (2004) 1656–1676.
- U. Essman, L. Perera, M.L. Berkowitz, T. Darden, H. Lee, L.G. Pedersen, A smooth particle mesh Ewald method, *J. Chem. Phys.* 103 (1995) 8577–8592.
- B. Hess, H. Bekker, et al., LINCS: a linear constraint solver for molecular simulations, *J. Comput. Chem.* 18 (1997) 1463–1472, 1997.
- S.A. Nose, Molecular-Dynamics method for simulations in the canonical ensemble, *Mol. Phys.* 52 (1984) 255–268.
- W.G. Hoover, Canonical dynamics, equilibrium phase-space distributions, *Phys. Rev.* 31 (1985) 1695–1697.
- M. Parrinello, A. Rahman, Polymorphic transitions in single-crystals - a new Molecular-Dynamics method, *J. Appl. Phys.* 52 (1981) 7182–7190.
- D. Poger, A.E. Mark, On the validation of molecular dynamics simulations of saturated and cis-monounsaturated phosphatidylcholine lipid bilayers: a comparison with experiment, *J. Chem. Theor. Comput.* 6 (2010) 325–336.
- A.J. P. Neto, R.M. Cordeiro, Molecular simulations of the effects of phospholipid and cholesterol peroxidation on lipid membrane properties, *Biochim. Biophys. Acta Biomembr.* 1858 (2016) 2191–2198.
- D. Petrov, C. Margreitter, M. Grandits, C. Oostenbrink, B. Zagrovic, A systematic framework for molecular dynamics simulations of protein post-translational modifications, *PLoS Comput. Biol.* 9 (2013), e1003154.
- R.M. Cordeiro, Reactive oxygen and nitrogen species at phospholipid bilayers: peroxynitrous acid and its homolysis products, *J. Phys. Chem. B* 122 (2018) 8211–8219.
- R.M. Cordeiro, M. Yusupov, J. Razzokov, A. Bogaerts, Parametrization and molecular dynamics simulations of nitrogen oxyanions and oxyacids for applications in atmospheric and biomolecular sciences, *J. Phys. Chem. B* 124 (2020) 1082–1089.
- M.J. Frisch, G.W. Trucks, H.B. Schlegel, G.E. Scuseria, M.A. Robb, J.R. Cheeseman, G. Scalmani, V. Barone, B. Mennucci, G.A. Petersson, H. Nakatsuji, M. Caricato, X. Li, H.P. Hratchian, A.F. Izmaylov, J. Bloino, G. Zheng, J.L. Sonnenberg, M. Hada, M. Ehara, K. Toyota, R. Fukuda, J. Hasegawa, M. Ishida, T. Nakajima, Y. Honda, O. Kitao, H. Nakai, T. Vreven, J.A. Montgomery Jr., J.E. Peralta, F. Ogliaro, M. Bearpark, J.J. Heyd, E. Brothers, K.N. Kudin, V.N. Staroverov, T. Keith, R. Kobayashi, J. Normand, K. Raghavachari, A. Rendell, J.C. Burant, S.S. Iyengar, J. Tomasi, M. Cossi, N. Rega, J.M. Millam, M. Klene, J.E. Knox, J.B. Cross, V. Bakken, C. Adamo, J. Jaramillo, R. Gomperts, R.E. Stratmann, O. Yazyev, A. J. Austin, R. Cammi, C. Pomelli, J.W. Ochterski, R.L. Martin, K. Morokuma, V. G. Zakrzewski, G.A. Voth, P. Salvador, J.J. Dannenberg, S. Dapprich, A.D. Daniels, O. Farkas, J.B. Foresman, J.V. Ortiz, J. Cioslowski, D.J. Fox, Gaussian 2009, Revision D.01, Gaussian, Inc., Wallingford CT, 2013.
- A. Leftin, T.R. Molugu, C. Job, K. Beyer, M.F. Brown, Area per lipid and cholesterol interactions in membranes from separated local-field <sup>13</sup>C NMR spectroscopy, *Biophys. J.* 107 (2014) 2274–2286.
- G. Weber, T. Charitat, et al., Lipid oxidation induces structural changes in biomimetic membranes, *Soft Matter* 10 (2014) 4241–4247.
- L. Beranova, L. Cwiklik, et al., Oxidation changes physical properties of phospholipid bilayers: fluorescence spectroscopy and molecular simulations, *Langmuir* 26 (2010) 6140–6144.
- E. Parra-Ortiz, K.L. Browning, L.S.E. Damgaard, et al., Effects of oxidation on the physicochemical properties of polyunsaturated lipid membranes, *J. Colloid Interface Sci.* 538 (2019) 404–419.
- S. Kumar, R. Rana, D.K. Yadav, Atomic-scale Modeling of the Effect of Lipid Peroxidation on the Permeability of Reactive Species, 2020, <https://doi.org/10.1080/07391102.2020.1730971>.

- [45] M.C. Oliveira, M. Yusupov, A. Bogaerts, R.M. Cordeiro, Molecular dynamics simulations of mechanical stress on oxidized membranes, *Biophys. Chem.* 254 (2019) 106266.
- [46] I.O.L. Bacellar, M.C. Oliveira, L.S. Dantas, et al., Photosensitized membrane permeabilization requires contact-dependent reactions between photosensitizer and lipids, *J. Am. Chem. Soc.* 140 (2018) 9606–9615.
- [47] R.M. Cordeiro, Molecular dynamics simulations of the transport of reactive oxygen species by mammalian and plant aquaporins, *Biochim. Biophys. Acta Gen. Subj.* 1850 (2015) 1786–1794.
- [48] S. Marrink, H.J.C. Berendsen, Simulation of water transport through a lipid membrane, *J. Phys. Chem.* 98 (1994) 4155–4168.
- [49] R.M. Cordeiro, Molecular structure and permeability at the interface between phase-separated membrane domains, *J. Phys. Chem. B* 122 (2018) 6954–6965.
- [50] M. Yusupov, D. Yan, R.M. Cordeiro, A. Bogaerts, Atomic scale simulation of H<sub>2</sub>O<sub>2</sub> permeation through aquaporin: toward the understanding of plasma cancer treatment, *J. Phys. Appl. Phys.* 51 (2018) 125401.